Defects in BaMgAl$_{10}$O$_{17}$: Eu^{2+} Blue Phosphor

ZHEHUA WU & A.N. CORMACK*

School of Ceramic Engineering and Materials Science at Alfred University

Abstract. The luminescent properties of BaMgAl$_{10}$O$_{17}$: Eu^{2+} blue phosphor are closely related to the valence state of europium inside the crystal and its defect structure. Because of the complexity of the BAM structure, research was carried out to study the europium-related defects by computer simulation. Two different Mg distributions were found to have the same lattice energy, but the arrangement of Mg affected the defect energy and Eu position. Eu^{3+} behavior was also discussed to address the oxidation-induced luminescent degradation. Two energetically most-favorable positions were found for europium, depending on the oxidation state: the Beevers-Ross site on the conduction plane for Eu^{2+}, and the Al(2) site in the middle of the spinel block for Eu^{3+}. Results of defect complex and bond-valence calculations suggested that the large europium ion can reside in the oxygen close-packed spinel blocks. A comparison of europium defect properties calculated with two different potential models suggests that results of the simulations are potential independent.

Keywords: BAM, phosphor material, Eu incorporation, computer simulation

Introduction

The optical properties of phosphor materials depend not only on the active elements but also on the host materials. The active ions, typically rare-earth ions, are introduced into the host material as dopants. The local environment of the active element will change the emission spectrum of the final phosphor material. In an increasing number of cases, host compounds have somewhat complex crystal structures, which provide several possible sites for the active ion.

BaMgAl$_{10}$O$_{17}$(BAM):Eu^{2+} is widely used as a blue phosphor for lamp and display panels. However, it is not clear where the exact positions of europium ions are in the structure, from experiment because of the complex crystal chemistry of BAM structure. Computer simulations, on the other hand, have been found to be a successful approach to a wide range of defect studies.

In this paper, various aspects of barium β-aluminates (BAM) have been investigated with the aid of computer simulation; these include the BAM structure itself, magnesium distributions and defect properties. Besides the europium extrinsic defects, intrinsic defects have also been studied because they affect charge compensating mechanisms when europium ions are introduced into the structure. The potential dependence of the results has also been investigated.

Detail of Structure

The BAM structure is derived from that of β-alumina (NaAl$_{11}$O$_{17}$) which was first discovered by Rankin and Merwin [1–3]. Bragg, and Beevers and Ross refined the β-alumina structure with x-ray diffraction; the atom positions are summarized in Table 1 [4, 5]. The structure has a space group of P6$_3$/mmc and can be described as consisting of oxygen close-packed spinel blocks of composition [Al$_{11}$O$_{16}$]$^{+1}$ separated by mirror planes of composition [NaO]$^{-1}$ (Fig. 1). The stacking order of oxygen close-packed layers in one spinel block is ABCA. Sodium occupies the Beevers-Ross (BR) site in the mirror plane. Aluminum ions occupy both octahedral and tetrahedral sites in the spinel

*To whom all correspondence should be addressed. E-mail: Cormack@alfred.edu

Table 1. Crystallographic information for the β-alumina structure **a** = 5.594 Å **c** = 22.53 Å

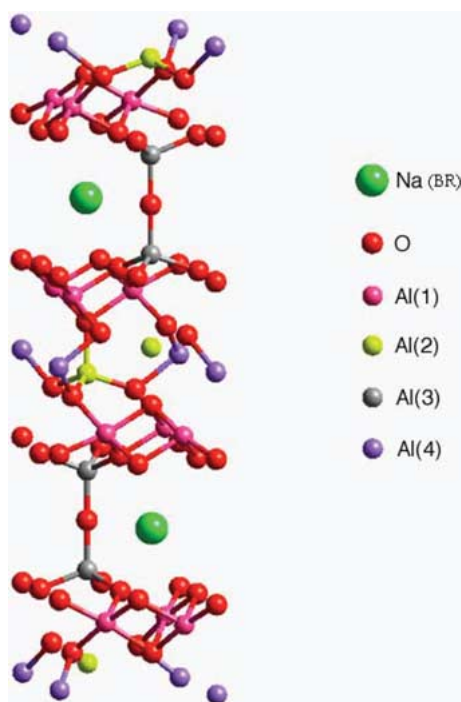| Atom	Wyckoff position	Type of site	x	y	z
Na(1)	2c	BR	2/3	1/3	1/4
Al(1)	12k	Octahedral	0.832	$-x$	0.106
Al(2)	4f	Tetrahedral	1/3	2/3	0.025
Al(3)	4f	Tetrahedral	1/3	2/3	0.176
Al(4)	2a	Octahedral	0	0	0
O(1)	12k	Tetrahedral	0.157	$-x$	0.05
O(2)	12k	Tetrahedral	0.503	$-x$	0
O(3)	4f	Tetrahedral	1/3	2/3	0.056
O(4)	4e	Tetrahedral	0	0	0.143
O(5)	2c	Tetrahedral	1/3	2/3	1/4

Fig. 1. Primitive cell of β-alumina.

block. Based on the symmetry, there are 4 aluminum, 5 oxygen and 1 sodium in symmetrically independent positions. In forming BAM, sodium is replaced by barium and the same number of aluminum ions is replaced by magnesium in order to keep the unit cell charge neutral. Thus the chemical formula of the spinel blocks becomes $[MgAl_{10}O_{16}]$ and the mirror plane changes to $[BaO]$; both are charge neutral. Magnesium may substitute in any of the four aluminum sites in the crystal

but the structure will be more stable if the original symmetry is kept as far as possible after the substitution, as shown in our simulations. Because the spinel blocks are similar to the structure of $MgAl_2O_4$ and Mg occupies the tetrahedral positions in spinel, the possible positions of Mg in the spinel blocks are most likely also to be the tetrahedral sites: Al(2) and Al(3).

The simulations in this study are based on the Born model description of a solid, which treats the solid as a collection of point ions with long-range and short-range forces acting between them. This approach has enjoyed a wide range of success, but it has been found that the reliability of the simulations depends on the validity of the potential model used in the calculations. The non-Coulombic potentials are usually described by a simple analytical Buckingham function,

$$V_{ij}(r_{ij}) = A_{ij} \exp(-r_{ij}/\rho_{ij}) - C_{ij}r_{ij}^{-6} \qquad (1)$$

where r_{ij} is the distance between the ions i and j.

The polarizability of the individual ion is included through the core-shell model originally developed by Dick and Overhauser, in which the outer valence electron cloud of the ion is simulated by a massless shell of charge Y and the nucleus and inner electrons by a core of charge X [6]. The total charge of the ion $(X + Y)$ is equal to the oxidation state of the ion. The interaction between core and shell of the same ion is harmonic with a spring constant k, and is given by

$$V_i(r_i) = \frac{1}{2}k_i d_i^2 \qquad (2)$$

where d_i is the relative displacement of core and shell of ion i.

For the core-shell model, the value of the free-ion electronic polarizability is given by

$$\alpha_i = Y_i^2/k_i. \qquad (3)$$

The potential parameters (A, ρ, and C in Eq. (1)), the shell charges Y, and the spring constant k associated with the shell-model description of polarizability need to be determined for the interactions between each ion pair in the crystal. In the present study, they were taken from our earlier studies of hexaaluminates following the original compilation of Lewis and Catlow [7–9]. Another set of potentials derived independently by Bush et al. was also tested [10].

Lattice Energy Calculations

The lattice energy is the binding or cohesive energy of the perfect crystal and is usually defined as the energy that must be released to the crystal to separate its component ions into free ions at rest at infinite separation. It is calculated by the relation:

$$U = 1/2 \sum \sum V_{ij}. \qquad (4)$$

The interatomic potential, V_{ij}, includes the long-range Coulombic interactions and the non-Coulombic potential described above. The lattice energy is minimized through a second derivative Newton-like procedure, coded into METAPOCS [11]. Details of the procedure have been outlined by Cormack [12].

In the present work, this perfect lattice approach has been used to establish an equilibrated crystal structure for BAM using the previously published potential summarized in Table 2 [7]. In addition, Bush potentials, shown in Table 3 were used to examine whether the results are potential independent.

Defect Energy Calculations

Calculations of defect structure and energy introduce one vital feature in addition to those for the perfect lattice methods. That is, the relaxation of lattice atoms around the defect species. The defect generally provides an extensive perturbation of the surrounding lattice, and, in the case of ionic crystals, the relaxation field is long-range as the perturbation provided by the defect is mainly Coulombic in origin.

The defect calculation is based on the Mott-Littleton theory, which allows one to calculate the defect-

Table 2. Potential parameters derived by Lewis and Catlow

Interaction	A (eV)	ρ (Å)	C (eV·Å^6)
Al(o)—O	1474.40	0.30059	0
Al(t)—O	1334.31	0.30059	0
Ba—O	931.70	0.39490	0
Mg—O	710.50	0.32420	0
O—O	22764.2	0.14910	17.89
Eu(2+)—O	665.20	0.39490	0
Eu(3+)—O	1358.0	0.35560	0
	Shell charge		K
Ba (core)—Ba (shell)	1.46		14.78
O(core)—O(shell)	−2.207		27.29

Table 3. Potential models derived by Bush et al.

Interaction	A (eV)	ρ (Å)	C (eV·Å^6)
Al—O	2409.505	0.2649	0
Ba—O	4818.416	0.3067	0
Mg—O	2457.243	0.2610	0
O—O	25.41	0.6937	32.32
Eu(2+)—O	6212.907	0.27948	0
Eu(3+)—O	847.868	0.3791	0
	Shell charge	Spring constant	
Al(core)—Al(shell)	2.957	403.98	
Ba(core)—Ba(shell)	1.831	34.05	
O(core)—O(shell)	−2.513	20.53	
Eu(3+ core)—Eu(3+ shell)	3.991	304.92	

induced static polarization of a dielectric continuum [13]. The basic approach is to contain, within the dielectric continuum, a region, immediately surrounding the defect, which is treated atomistically within the framework of the Born model described above. In this region, the forces and resulting atom displacements are too large to be treated properly using continuum theory, which can, nevertheless, be used to model the more distant parts of the crystal. This two-region approach is coded in CASCADE that was the program used in this work.

Results

Structures of BAM

Using β-alumina as a prototype, the BAM structure was obtained by substituting, in a primitive cell, both Na with Ba and two Al with Mg; the structure was then relaxed to a minimum energy configuration. Mg ions were put in Al(2) or Al(3) positions (four Al(2) positions are labeled as a–d and four Al(3) positions are labeled as a′–d′ along c axis in Fig. 2). It was determined that the lattice energy of the unit cell with all Mg in Al(2) sites was lower than for the other Mg distributions (Table 4). Furthermore, there are three possible ways to put two magnesium ions in four Al(2) sites.

After checking all the possibilities, in which magnesium ions are in ab, ac and bc sites respectively, two types of Mg distribution were found to have nearly the same lattice energy (just a 0.06 eV difference). This suggests that there will be a variety of Mg distributions in BAM crystals, since apart from the preference for
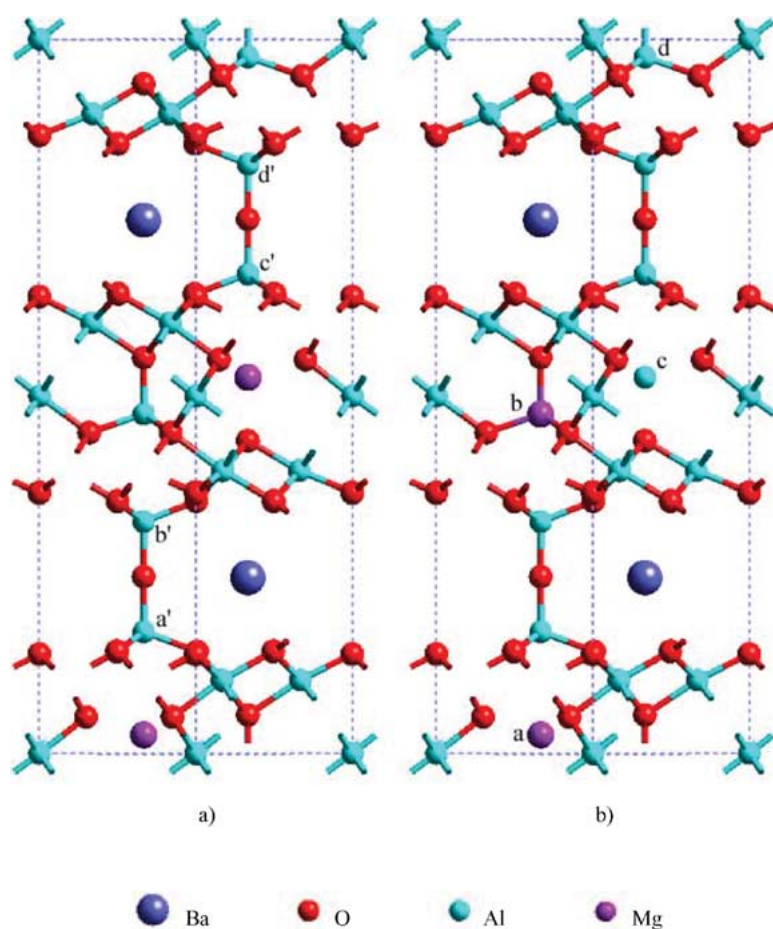
Fig. 2. Two configurations of BAM. (a) Configuration I possesses Mg at ab sites; (b) Configuration II possesses Mg at ac sites.

the Al(2) site there is no driving force for Mg ordering in the equivalent sites. These two possible structures of BAM have been defined as configuration I and II. Configuration I has Mg in a and c sites, and configuration II has Mg in a and b sites (Fig. 2). In configuration II, the two mirror planes in the unit cell are now different

Table 4. Lattice energies of Mg distributions in Al(2) and Al(3) sites

Configuration with Al(2) and Al(3) mix	aa'	ab'	ac'	ad'
Lattice energy (eV)	-1733.27	-1734.91	-1735.09	-1733.60
Configuration with only Al(2)	ab	ac	bc	
Lattice energy (eV)	-1736	-1736.06	-1733.83	
Configuration with only Al(3)	$a'b'$	$a'c'$	$b'c'$	
Lattice energy (eV)	-1733.32	-1734.42	-1733.71	

from each other because of the Mg distribution and then the defect properties may vary in different regions. In configuration II, all Mg are located in the lower half of the unit cell (IIM) and no Mg is in the upper half (IIA). Actually, configuration I has lost the mirror symmetry but kept the 2-fold screw axis, whereas configuration II has kept the mirror symmetry but lost the 2-fold screw axis. For convenience, the phrase "mirror plane" is generally used to refer to the barium-oxygen plane in both configurations.

The calculated crystal structure parameters for BAM (configuration I) are given in Table 5, in which they are compared with the experimental data of Iyi et al. [2]. Because the equilibrated structure changed slightly after the substitution of Mg, the coordinates are averaged over the symmetrically independent positions. In addition, the Mg in the spinel block was

Table 5. Comparison of measured and calculated structures

Atom type	$X_{obs.}$	$X_{calc.}$	ΔX	$Z_{obs.}$	$Z_{calc.}$	ΔZ
Ba	0.6678	0.6667	0.0011	0.2500	0.24662	0.00338
Al(1)	0.8343	0.8338	0.0005	0.10544	0.10268	0.00276
Al(2)	0.3333	0.3333	0	0.02400	0.01848	0.00552
Al(3)	0.3333	0.3333	0	0.17416	0.17052	0.00364
Al(4)	0.0000	0.0000	0	0.00000	0.00000	0
O(1)	0.1534	0.1488	0.0046	0.05152	0.05130	0.00022
O(2)	0.5042	0.5040	0.0002	0.14799	0.14333	0.00466
O(3)	0.6667	0.6667	0	0.05901	0.05409	0.00492
O(4)	0.0000	0.0000	0	0.14437	0.139590	0.00478
O(5)	0.3333	0.3333	0	0.25000	0.24789	0.00211

Table 6. Calculated point defect energies (eV)

Defect	Config. I	Config IIM	Config. IIA
V''_{Ba}	17.01	17.70	16.16
V''_{Mg}	29.30	29.39	29.39
$V'''_{Al(1)}$	58.34	58.66	56.78
$V'''_{Al(2)}$	58.52	–	58.31
$V'''_{Al(3)}$	59.39	59.78	58.92
$V'''_{Al(4)}$	57.08	57.07	57.07
$V^{\bullet\bullet}_{O(1)}$	23.31	23.18	24.90
$V^{\bullet\bullet}_{O(2)}$	24.92	24.62	26.00
$V^{\bullet\bullet}_{O(3)}$	25.44	25.47	25.62
$V^{\bullet\bullet}_{O(4)}$	23.33	23.13	25.79
$V^{\bullet\bullet}_{O(5)}$	25.16	24.02	26.23
$Ba^{\bullet\bullet}_{i}$	−11.21	−12.19	−10.25
$Mg^{\bullet\bullet}_{i}$	−18.22	−18.91	−16.94
$Al^{\bullet\bullet}_{i}$	−42.51	−42.86	−42.57
O''_{i}	−14.76	−15.52	−15.24

introduced as a defect, and the lattice must relax in some way to allocate the defect. This relaxation changes the size and shape of the spinel block slightly; that is the reason for the fact that Ba and O(5) ions did not remain exactly on the mirror plane ($z = 0.25$, 0.75). Having magnesium and barium in the structure has expanded the unit cell and the cell parameters become **a** = 5.72Å and **c** = 22.65Å. Although the calculated structure is technically slightly different from the β-alumina structure, the agreement between our modeled structure and the experiment data of BAM is very good, as can be seen from the Δx and Δz columns in Table 5, which represents the difference between calculation and experiment.

Because of the good agreement between calculated and measured structural data, the potential was ready for further defect simulations. Although the Mg distribution does not affect the lattice energies significantly for configurations I and II, they may be expected to have a significant effect on the energies of point defects.

Intrinsic Disorder

Point defect energies of all ion species in the two configurations and the two regions of configuration II have been calculated and are compared in Table 6. These are the energies associated with bringing the defects into the crystal from infinity. No ionization processes have been included. As the introduction of Mg into the structure has changed the symmetry, defect energies in BAM will not necessarily be the same for the originally symmetry-similar positions of β-alumina. It is thus appropriate to calculate defects on all possible lattice sites as well as sites that are normally symmetrically equivalent. For example, all vacancies on Al(2) sites in β-alumina should have the same defect energy.

But in BAM, the aluminum ions in the Al(2) position have different environments compared to each other; i.e. one Al(2) would have a magnesium close to it but the other has magnesium further away. Although their environments, or site symmetries, are different, they are still described as being in the Al(2) position, as classified in β-alumina, to keep the discussion simple. Thus all aluminums in the Al(2) sites must be calculated individually. When looking at the Table 6, it must be kept in mind that the defect energy listed was the lowest one for that class of positions.

When considering the interstitial defect, one will wonder where are the possible interstitial positions for ions. Since the mirror plane region is quite open in β-alumina and symmetry has been impaired, it is not so straightforward to select all the possible positions, besides the special sites such as unoccupied octahedral sites and the anti-BR site. In order to consider all of the possibilities, a computer program was designed to find the possible positions automatically. The basic idea of the program is that as long as the site is large enough (i.e. the distance from this site to its nearest ion is larger than a prescribed threshold), it can be a candidate to hold an interstitial ion. The smaller is the size of the interstitial position, the bigger the relaxation needed to accommodate the interstitial ion, and the higher the defect energy may be, and more sites will be selected. No distance between two interstitial positions was allowed to be shorter than the threshold, to limit the number of selected sites. Another criterion is that no two sites will have the same immediate environment. Even though many limitations have been applied to the

structure, the program still generated around 200 candidate sites. The lower the symmetry, the more candidates are generated. All of the generated interstitial sites have been tested for each ion species and the position with the lowest point defect energy has been considered as the interstitial position for that ion species. However, that does not mean interstitials only occur at that position; it merely means that the probability of finding an interstitial of that ion at that position is the greatest.

In configuration I, the aluminum vacancy seems most likely to occur at Al(4) in the middle of spinel block, but it was the Al(1) site that would be preferred in configuration II. Other vacancy positions were found to be the same for the two Mg distributions.

The barium interstitial prefers to occupy the anti-BR site in the mirror plane (see Fig. 3) and was the same for both configurations. Since the divalent barium ion is quite large relative to other ions (its radius is 1.5 Å, which is nearly double the size of an aluminum ion), it is not surprising that barium can not reside inside the spinel block since it is oxygen close-packed, without additional defect creation (see Park and Cormack). Magnesium was also found to occupy the anti-BR site, but with a little deviation toward a nearby O(5) ion. Aluminum behaves differently from other cations because its size is so small that it can enter into the spinel

block. Aluminum ion prefers to take the octahedral sites across the middle of the spinel block. Since there are three cation layers in the middle of a spinel block, Mg—Al(4)—Al(2), two oxygen layers at the edge of this region have been separated further away from each other, and they are no longer strictly close-packed. The octahedron formed by these two oxygen layers has become distorted and longer in the **c** direction. The aluminum interstitial was not found in the center of the octahedron but closer to the Al(2) layer, because of the relaxation around magnesium ion. The fact that aluminum interstitial ions are inside the spinel blocks is consistent with the observation of neutron diffraction by Roth et al. [14]. Oxygen interstitials in configuration I sit in the Al(1) layer and close to the unoccupied octahedral site; this is different from the observation in β-alumina [15].

For oxygen in β-alumina, the favorite interstitial position is the mO site in the conduction plane, between two adjacent O(5) ions. After relaxation, two Al(1) ions above and below the mO site move automatically toward the conduction plane to stabilize the interstitial ion. This creates a V_{Al}—Al_i—O_i—Al_i—V_{Al} defect cluster, called a Reidinger defect, across the mirror plane (see Fig. 4(a)). The interstitial oxygen stayed strictly on the mirror plane. After its migration, the coordination number of the aluminum in the
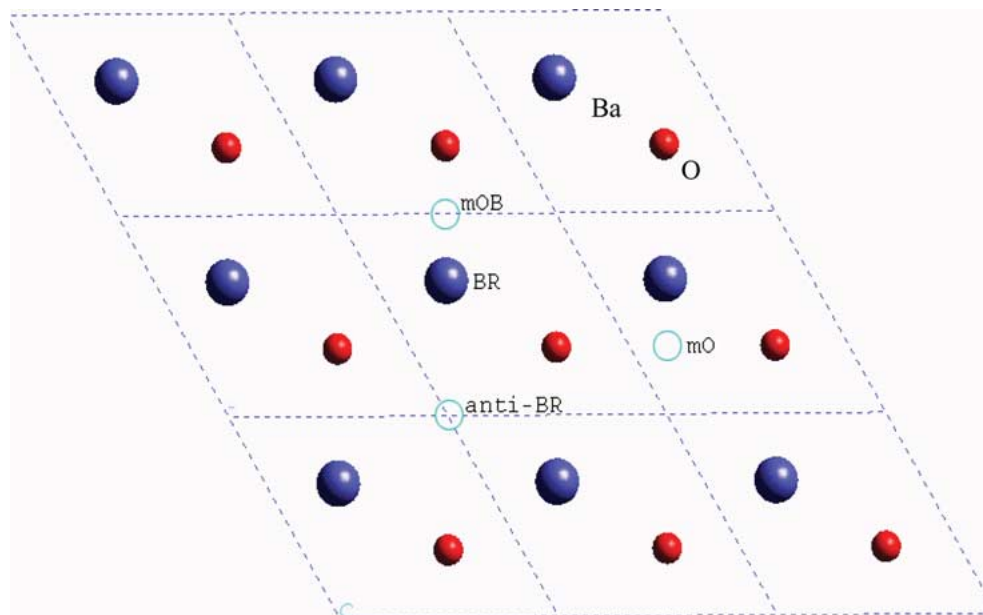

Fig. 3. Projection of mirror plane of BAM with ion positions at X-Y plane.
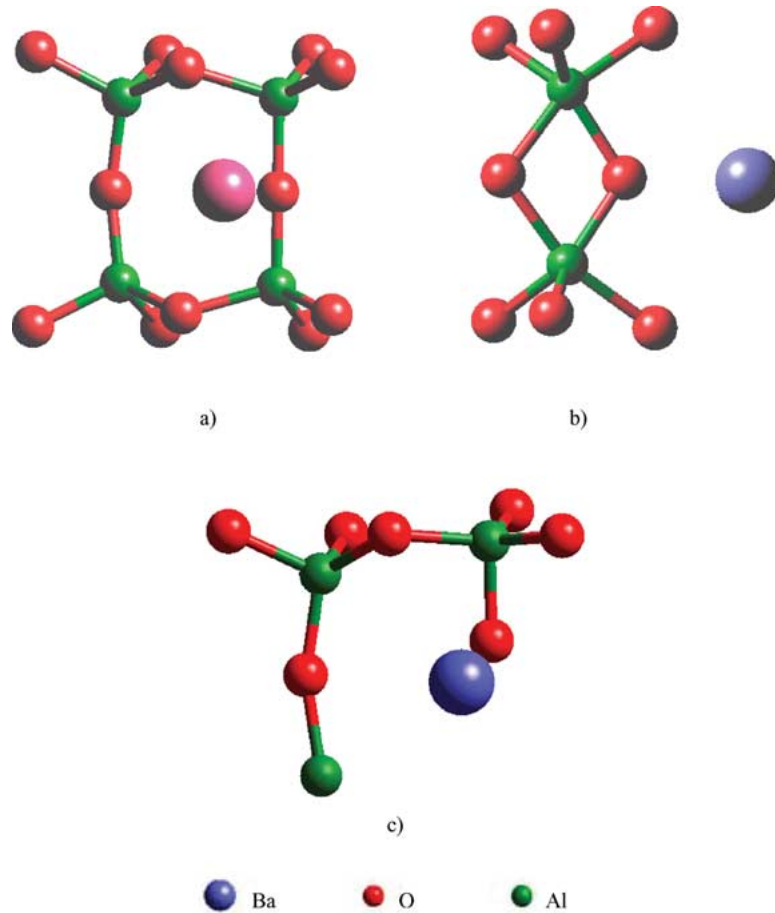
Fig. 4. Three types of oxygen interstitial of BAM.

Reidinger defect changes from six to four. However, for configuration I of BAM, only one aluminum ion moved toward the O$_I$, forming a V$_{Al}$—Al$_i$—O$_i$ defect cluster (Fig. 4(c)) if the oxygen interstitial ion was put into the mO position. In this case the interstitial oxygen no longer stayed on the mO site but relaxed away from the nearby barium and the mirror plane. The reason is that barium is larger than sodium so the oxygen interstitial is pushed away and the two corner-shared tetrahedra of the Reidinger defect become bent and stretched. Then, the Reidinger defect was no longer stable, and it broke. However, oxygen can still be stabilized by a single aluminum ion moving toward it. Therefore, the defect energy for the oxygen interstitial in the mirror plane is no longer the lowest one, even if forcing the structure to form a Reidinger defect before the defect relaxation.

Another kind of defect cluster of oxygen interstitials has been found in configuration II. The oxygen interstitial ion tends to stay between the barium and a nearby O(5) ion that normally associates with two Al(3) ions to form a bridge perpendicular to the mirror plane; this position is defined as the mOB site. The O(5) ion shared the aluminum ions with the interstitial oxygen and formed a two-bridge configuration. The Al(3)—O(5)—Al(3)—O$_i$ defect cluster forms a parallelogram (see Fig. 4(b)). It should be mentioned that this parallelogram is mirror symmetric across the conduction plane. That is the reason why this defect has the lowest defect energy, for it keeps the symmetry of the configuration II structure. While testing this two-bridge configuration in configuration I, the defect energy was found to be −14.23 eV, a little higher than the lowest one found earlier. It is not surprising to see this because the structure of configuration I has no mirror symmetry, so the two-bridge defect-cluster with mirror symmetry has no benefit over other defects.
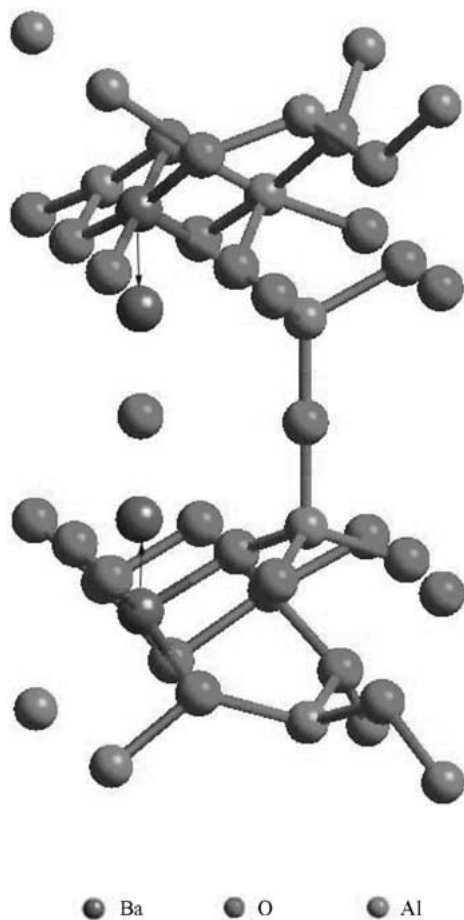
● Ba   ● O   ● Al

Fig. 5. Configuration of Reidinger defect.

The chemical formula of region IIM is $[BaMg_2Al_9O_{17}]^{-1}$ while the formula of region IIA is $[BaAl_{11}O_{17}]^{+1}$. It is reasonable to suppose that a net-positive-charged point defect should prefer the IIM region and vice versa; this proves to be true in the calculation.

Energies of Schottky and Frenkel defects have been calculated from the point defect energies [16]. These intrinsic defect energies have been normalized (per defect) for comparison. A Frenkel defect consists of one vacancy and one interstitial point defect while the Schottky defect consists of a formula unit of vacancies.
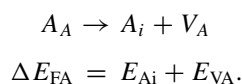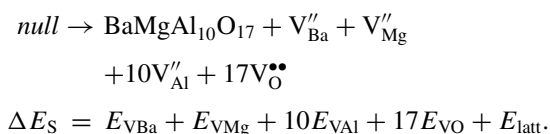
The Frenkel defect energy calculations involve

$$A_A \rightarrow A_i + V_A$$
$$\Delta E_{FA} = E_{Ai} + E_{VA}.$$

Table 7. Calculated intrinsic defect energies (eV)

Disorder	Config. I	Config. IIM	Config. IIA	Lowest
Schottky	5.01	4.93	5.82	4.93
Frenkel: O	4.28	3.81	4.83	3.81
Frenkel: Ba	2.90	2.76	2.96	2.76
Frenkel: Mg	5.54	5.24	6.23	5.24
Frenkel: Al	7.29	7.11	7.11	7.11

The Schottky defect energy calculations involve

$$null \rightarrow BaMgAl_{10}O_{17} + V''_{Ba} + V''_{Mg}$$
$$+ 10V''_{Al} + 17V^{\bullet\bullet}_O$$
$$\Delta E_S = E_{VBa} + E_{VMg} + 10E_{VAl} + 17E_{VO} + E_{latt}.$$

In order to compare different defects, the intrinsic defect energy was calculated per single point defect. Table 7 lists the final comparable defect energies. The barium Frenkel defect has the lowest defect energy, and, therefore, will be predominant in thermally generated defects. The energetically favorable barium interstitial position is the anti-BR site on the mirror plane. In addition, point defects will be created for charge compensation after the introduction of europium or other optically active ions.

Europium Incorporation

It is important to determine the sites of europium ion to understand the luminescent behavior of BAM phosphor. There are many processes available for Eu to enter into the structure, and the way to distinguish between them lies in the heat of solution; the incorporation process with the lowest heat of solution will be the one that dominates. The Eu ion may substitute for cations or enter into interstitial sites. First, the sites with lowest defect energy were found (see Table 8) while allocating Eu to where it could possibly reside. The second step was to write down the solution reaction.

The defect energies in Table 8 are the lowest one for each kind of defect. For example, Eu^{2+} ions can substitute for the different Al ions in different symmetry locations. There is no doubt that four different defect energies will be obtained. Here the defect energy of Eu'_{Al} corresponds to the one of Eu^{2+} ions substituting for the Al(2) ion since it has the lowest point defect energy. There was no difference in the positions of the europium defect for the two structural configurations.

Table 8. Europium point defect energies (eV)

Defect	Config. I	Config. II
Eu$_{Ba}$	−1.34	−1.47
Eu$_{Mg}$	10.59	10.59
Eu$'_{Al}$	38.47	38.34
Eu$_i^{\bullet\bullet}$	−12.88	−14.00
Eu$_{Ba}^{\bullet}$	−21.67	−22.22
Eu$_{Mg}^{\bullet}$	−13.23	−13.29
Eu$_{Al}$	14.44	14.37
Eu$_i^{\bullet\bullet\bullet}$	−31.56	−33.32

Table 10. Eu^{3+} ion incorporation into BAM

Defect reaction	Enthalpy (eV) Conf. I	Enthalpy (eV) Conf. II
1/2Eu$_2$O$_3$ → Eu$_i^{\bullet\bullet\bullet}$ + 3/2O$''_i$	11.74	8.84
1/2Eu$_2$O$_3$ → Eu$_{Al}$ + Al$_i^{\bullet\bullet\bullet}$ + 3/2O$''_i$	15.23	13.66
1/2Eu$_2$O$_3$ → Eu$_{Al}$ + 1/2Al$_2$O$_3$	0.49	0.42
1/2Eu$_2$O$_3$ → Eu$_{Mg}^{\bullet}$ + MgO + 1/2O$''_i$	4.39	3.95
1/2Eu$_2$O$_3$ → Eu$_{Ba}^{\bullet}$ + BaO + 1/2O$''_i$	5.08	4.15

Lattice Energy (eV): E_{BaO} = −31.31; E_{MgO} = −40.99; E_{EuO} = −33.2; $E_{Al_2O_3}$ = −158.78; $E_{Eu_2O_3}$ = −130.88.

Interstitial ions were located on the anti-BR site. The Al(2) ion was easy to be substituted by the europium ions. Since there is only one kind of position each for Ba and Mg, there is no ambiguity in their substitution by europium.

The absolute value of the point defect energy is itself meaningless except for the comparison between the same kind of defects (such as interstitials). There is no way to tell which kind of defect will occur more easily than the others from the point defect energy alone unless they are put into a defect reaction and reaction enthalpies are calculated. The quasi-defect reactions, along with the corresponding reaction energies, or heats of solution, are shown in Tables 9 and 10.

It has been shown that the barium Beevers-Ross site is the most energetically favorable site for Eu^{2+} ion. This is most likely because mirror plane is more open than inside the spinel block and the doping process requires only a straight swap of barium for europium. The other possible mechanisms require a compensating defect, which will raise the overall energy of the defect reaction. Note that for interstitial Eu^{2+}, a barium vacancy could be an alternative compensating defect. If Eu$_i^{\bullet\bullet}$ and V$''_{Ba}$ are close to each other, the Eu$_i^{\bullet\bullet}$ will relax into the adjacent vacancy, which gives a simple swap process. Otherwise, the overall energy is somewhat higher.

Oxidation, a detrimental process for BAM phosphors, changes the valence of europium from 2 to 3. It is important to understand whether (or to what extent) the behavior of trivalent europium differs from divalent Eu. In a similar way, incorporation reactions for Eu^{3+} are written as shown in Table 10.

The important thing that should be noted is that the trivalent europium ion no longer prefers to substitute for the barium ion, as the divalent europium ion did. Instead it would prefer to substitute for an aluminum ion in the Al(2) position, that is, a tetrahedral site. This raises a potential problem in that conventional wisdom argues that it should not be possible for the large Eu^{3+} ion to sit between close-packed oxygen layers. As can be seen in Table 10, the substitution of barium by Eu^{3+} ions needs half the number of oxygen interstitials to compensate the charge generated. However, we should ask what would happen if the europium and oxygen ions were associated with each other. Would the association of O ions stabilize the Eu^{3+} ions at the BR site? Further simulations have been performed to investigate this kind of interaction between point defects.

Table 9. Eu^{2+} ion incorporation into BAM

| Defect reaction	Enthalpy (eV) Conf. I	Enthalpy (eV) Conf. II
EuO → Eu$_i^{\bullet\bullet}$ + O$''_i$	5.56	3.68
EuO → Eu$'_{Al}$ + Al$_i^{\bullet\bullet\bullet}$ + O$''_i$	14.4	13.16
EuO → 1/2Al$_2$O$_3$ + Eu$'_{Al}$ + 1/2V$_O^{\bullet\bullet}$	3.94	3.72
EuO → Eu$_{Mg}$ + Mg$_i^{\bullet\bullet}$ + O$''_i$	10.81	9.36
EuO → MgO + Eu$_{Mg}$	3.35	2.35
EuO → BaO + Eu$_{Ba}$	0.55	0.42
EuO → Eu$_i^{\bullet\bullet}$ + V$''_{Ba}$ + BaO	6.02	4.05

Defect Complexes

When two defects are placed close to each other, they interact and may decrease or increase the total defect energy. A complex is effectively formed when the interaction energy lowers the overall energy of the system. Defect complexes in the mirror plane containing europium ions were modelled. It has been shown above that the divalent europium ion would occupy the mirror plane and that the trivalent ion would be found close to the middle of the spinel block. In the mirror

Table 11. Defect complexes containing Eu^{3+} and O^{2-}

Oxygen position	Europium position	Config. I (eV)	Config. II (eV)
mO	BR	−36.79	–
mO	Anti-BR	−50.38	−50.25
mOB	BR	−39.06	−39.47
mOB	Anti-BR	−51.96	−52.92

plane, two positions were available for europium ions: the Beevers-Ross and anti-Beevers-Ross sites. Also, two positions have been found for oxygen interstitial ions: mO and mOB sites (see Fig. 3). Defect complexes with two point defects were calculated first (Table 11). The two point defects were placed as close as possible to get the maximum interaction.

The formation of defect complexes did lower the defect energy. For example, in configuration I,

$$Eu_{Ba}^{\bullet} + O_i'' \rightarrow (Eu_{Ba}^{\bullet} + O_i'')$$

$$\Delta H = -36.79 + 14.76 + 21.67 = -0.36 \, eV.$$
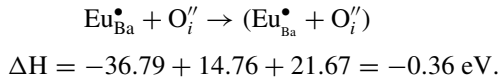
The Eu^{3+} and O interstitials came close to each other and that lowered the defect energy by 0.36eV. If the decrease in the defect energy were to be large enough, it might be possible for Eu^{3+} ions to remain in the mirror plane.

Defect complexes with three point defects have also been considered. BR and anti-BR sites were occupied by europium at the same time while oxygen interstitials were put into mO or mOB sites. The association of divalent and trivalent europium ions was also calculated in Table 12.

The more complicated defect complexes were energetically unfavorable because they generated big dipole moments in a small region that resulted in a large

Table 12. Defect complexes with three point defects

Defect complex	Config. I (eV)	Config. II (eV)
$Eu_{Ba}^{\bullet} - O_i'' (mO) - Eu_i^{\bullet\bullet\bullet}$	−73.83	−75.03
$O_i'' (mOB) - Eu_{Ba}^{\bullet} - Eu_i^{\bullet\bullet\bullet}$	−70.54	−71.92
$Eu_{Ba}^{\bullet} - Eu_i^{\bullet\bullet\bullet} - O_i'' (mOB)$	−73.12	−74.47
$Eu_{Ba} - O_i'' (mO) - Eu_i^{\bullet\bullet\bullet}$	−52.23	−52.28
$O_i(mOB) - Eu_{Ba} - Eu_i^{\bullet\bullet\bullet}$	−49.00	−50.00
$Eu_{Ba} - Eu_i^{\bullet\bullet\bullet} - O_i'' (mOB)$	−53.44	−54.39
$Eu_{Ba}^{\bullet} - O_i'' (mO) - Eu_i^{\bullet\bullet}$	−53.12	−52.93
$O_i'' (mOB) - Eu_{Ba}^{\bullet} - Eu_i^{\bullet\bullet}$	−51.76	−52.52
$Eu_{Ba}^{\bullet} - Eu_i^{\bullet\bullet} - O_i'' (mOB)$	−52.07	−52.82

stress in their surroundings. For example, a O_i'' (mOB) - $Eu_{Ba}^{\bullet} - Eu_i^{\bullet\bullet\bullet} - O_i''$ (mOB) complex had a defect energy of −90.82 eV, less negative than the sum of the energies of the two separated defect complexes, O_i'' (mOB) $-Eu_{Ba}^{\bullet}$ and $Eu_i^{\bullet\bullet\bullet} - O_i''$ (mOB), −91.02 eV. And, the association between defects in a big defect complex would become weaker because of the larger separation of point defects from one end to the other.

Based on the defect reaction enthalpies in Table 13, defect complexes cannot constrain the trivalent europium ion to the mirror plane, for either structural configuration. Although forming defect complexes sometimes lowers the reaction enthalpy, the decrease is not big enough: the enthalpy of forming the defect complex is still much larger than for europium substituting for Al(2). Thus, defect complexes cannot prevent the trivalent europium ion from entering into the tetrahedral Al(2) sites in the spinel block.

Europium Ion Size Consideration

Although it seems that the large Eu^{3+} ion should not reside in the spinel block because the spinel block is oxygen close-packed, the distance between two oxygen layers across the middle of spinel block (2.431 Å) is larger than distance between other neighboring oxygen layers (2.016 Å) in the spinel block. Therefore, the mid-region of the spinel block is not strictly close-packed. There are three cation-layers, Mg-Al(4)-Al(2), in the middle of the spinel block. Normally, the coordination number of rare-earth elements is at least six, because they are large in size and they prefer to reside in the larger sites. Thus, there is not much information about the Eu^{3+} radius in tetrahedral sites in the literature. However, it can be calculated from bond-valence theory and then can be compared with the distances in the calculated structure. Based on bond valence theory, the valence of an ion is related to its bond length with the form [17]

$$V_i = \sum_j v_j = \sum_j \exp\left(\frac{R_{ij} - d_{ij}}{b}\right) \qquad (5)$$

where V_i, the valence of ion i, is the summation of bond valences v_i between the central ion and its neighbors. d_{ij} is the bond length, R_{ij} is the bond valence parameter for the ion pair (i, j) and b is a constant equal to 0.37 [18]. The Eu^{3+}—O distances were 2.144 Å × 3 and 2.111 Å when the Eu^{3+} ion was in its preferred

Table 13. Defect reaction of defect complex

Defect reaction	Enthalpy (eV) Config. I	Enthalpy (eV) Config. II
$1/2Eu_2O_3 \rightarrow (Eu_i^{\bullet\bullet\bullet} + O_i'')_{com} + 1/2O_i''$	6.10	4.76
$1/2Eu_2O_3 \rightarrow (Eu_{Ba}^{\bullet} + O_i'')_{com} + BaO + 1/2V_O^{\bullet\bullet}$	6.72	6.22
$1/2Eu_2O_3 \rightarrow 1/2(Eu_i^{\bullet\bullet\bullet} + O_i'' + Eu_{Ba}^{\bullet})_{com} + 1/2BaO + 1/2O_i''$	5.49	4.51
$1/2Eu_2O_3 + EuO \rightarrow (Eu_i^{\bullet\bullet\bullet} + O_i'' + Eu_{Ba})_{com} + BaO + 1/2O_i''$	6.51	5.18
$1/2Eu_2O_3 + EuO \rightarrow (Eu_i^{\bullet\bullet} + O_i'' + Eu_{Ba}^{\bullet})_{com} + BaO + 1/2O_i''$	6.83	6.64

com: Defect complex.

Al(2) tetrahedral site. The bond valence sum for that position is calculated to be 3.389 (see Table 14) and is close to the europium oxidation state of 3; the 13% difference is in the reasonable range, compared to other ions. It seems that the Eu^{3+} ion has a bond valence just higher than the theoretical value, which means that Eu^{3+} ions will be tightly pinned by the environment and will hardly move. In contrast, those ions in the mirror plane, which can move easily, have bond valences far below their ideal values.

If it is assumed that all Eu^{3+}─O lengths are the same in a tetrahedron, Eq. (5) can be rewritten as:

$$d_{ij} = R_{ij} + b \ln\left(\frac{n}{V_i}\right) \qquad (6)$$

where n is the coordination number. This gives (Table 15) the predicted bond length for different coordination conditions.

The bond length of Eu^{3+}─O in BAM is smaller than the predicted value from bond valence theory. This may be related to the cation rich environment in the

Table 14. Cation bond valences

Ion	V_i	n	V_i/V_0 (%)
Al(1)	2.966	6	98.9
Al(2)	2.564	4	85.5
Al(3)	2.827	4	94.2
Al(4)	2.624	6	87.5
Ba	1.413	9	70.7
Mg	1.955	4	97.8
Eu^{2+}(BR)	1.071	9	53.6
Eu^{3+}(Al2)	3.389	4	113

V_0: theoretical valence.

Table 15. Bond length vs. coordination number

n (Eu-O)	4	5	6
d (Eu-O) Å	2.1804	2.263	2.3305

mid-spinel region. The oxygen ions around Eu^{3+} can not relax too much. Before the substitution, the Al─O bond lengths for Al(2) are 1.797 Å and 1.822 Å × 3. The substitution did relax the surrounding oxygen ions to a suitable distance to accommodate the large Eu^{3+} ion. The shortened Eu^{3+}─O bond length is a compromise between normal bond length and the actual surroundings.

Calculations with the Bush Potential

The potentials used to generate the above results were taken from the work of Lewis and Catlow and adjusted from our earlier studies [9]. Further verification has been done by using another set of totally different potentials (derived by Bush et al. [10]) to model the structure. Bush et al. used the Shell Model for all cations, and their potential model might thus be considered to be more accurate. However, they did not define a Eu^{2+}─O potential in their work, so we fit this potential to the properties of EuO later, using their oxygen-oxygen potential. Because of the lack of available physical data, the fitted potential was not completely satisfactory. However, as with the earlier potential, two Mg distributions were also found with the new potential. Since the potential dependence of calculations was the main concern, only the data for configuration I calculated by the Bush potential are listed (see Table 16).

On substituting for aluminum, europium ions again preferred the Al(2) sites. The preferred positions of all defects were the same, except for the aluminum vacancy. Using the Bush potentials, it is the Al(2) position that has the lowest vacancy energy. The europium point defects occur at exactly the same places with both two sets of potentials.

The predominant intrinsic defect was the barium Frenkel defect for the Lewis and Catlow potential,

Table 16. Point defect in Config. I with Bush potential

Intrinsic point defect	Defect energy (eV)	Extrinsic point defect	Defect energy (eV)
V''_{Ba}	19.06	Eu_{Ba}	−1.58
V''_{Mg}	27.90	Eu_{Mg}	8.53
$V'''_{Al(1)}$	58.88	Eu'_{Al}	35.88
$V'''_{Al(2)}$	56.34	$Eu^{\bullet\bullet}_i$	−14.64
$V'''_{Al(3)}$	59.60	$Eu^{\bullet}_{Ba}$	−19.65
$V'''_{Al(4)}$	60.24	$Eu^{\bullet}_{Mg}$	−12.99
$V^{\bullet\bullet}_{O(1)}$	18.54	Eu_{Al}	14.53
$V^{\bullet\bullet}_{O(2)}$	20.83	$Eu^{\bullet\bullet\bullet}_i$	−31.28
$V^{\bullet\bullet}_{O(3)}$	19.96		
$V^{\bullet\bullet}_{O(4)}$	19.14		
$V^{\bullet\bullet}_{O(5)}$	25.16		
$Ba^{\bullet\bullet}_i$	−12.84		
$Mg^{\bullet\bullet}_i$	−19.34		
$Al^{\bullet\bullet}_i$	−47.31		
O''_i	−11.61		

which was expected, but the Schottky defect has the lowest reaction enthalpy with the Bush potential (Table 17).

Although the absolute values of reaction energies show small differences, Eu^{3+} ions entering into the Al(2) site and Eu^{2+} ions substituting for barium still consume the lowest energy (Table 18). Another interesting observation is that the Eu^{2+} substitution for Al(2), the favorite site for Eu^{3+}, has a dramatically decreased heat of solution (close to that of Eu^{2+} in the BR site), raising the possibility that Eu^{2+} may also occur inside the spinel block, contrary to the previous results with the original Lewis and Catlow potential. Since the fitting of the Eu^{2+}—O potential to the Bush O—O potential was not completely satisfactory, however, the results obtained from the Lewis & Catlow potentials may be considered to be more reliable: only one Eu^{2+} position is likely to exist.

The environment of the Eu^{3+} ion on the Al(2) site consists of three Eu^{3+}—O bonds with a bond-length equal to 2.102 Å and one Eu^{3+}—O bond-length equal to 2.098 Å. This is close to the configuration obtained

Table 17. Intrinsic defect energy of BAM with Bush potential

Disorder	Energy (eV)
Schottky	1.87
Frenkel: O	4.28
Frenkel: Ba	3.11
Frenkel: Mg	4.28
Frenkel: Al	4.52

Table 18. Incorporation of Eu into BAM (Bush potential)

Defect reaction	Enthalpy (eV)
$EuO \rightarrow Eu^{\bullet\bullet}_i + O''_i$	8.28
$EuO \rightarrow 1/2Al_2O_3 + Eu'_{Al} + 1/2V^{\bullet\bullet}_O$	0.93
$EuO \rightarrow MgO + Eu_{Mg}$	2.18
$EuO \rightarrow BaO + Eu_{Ba}$	0.54
$1/2Eu_2O_3 \rightarrow Eu^{\bullet\bullet}_i + 3/2O''_i$	15.87
$1/2Eu_2O_3 \rightarrow Eu_{Al} + 1/2Al_2O_3$	0.37
$1/2Eu_2O_3 \rightarrow Eu^{\bullet}_{Mg} + MgO + 1/2O''_i$	4.83
$1/2Eu_2O_3 \rightarrow Eu^{\bullet}_{Ba} + BaO + 1/2O''_i$	6.7

Lattice energy (eV): $E_{BaO} = -32.46$; $E_{MgO} = -40.99$; $E_{EuO} = -34.58$; $E_{Al_2O_3} = -157.6$; $E_{Eu_2O_3} = -129.28$.

with the original potential, but the size is a little smaller. From this comparison, it is clear that the europium ion positions are insensitive to the potentials.

Conclusions

Based on our calculations, the BAM structure may accommodate two Mg distributions that cannot be distinguished by their lattice energies. We think both configurations will exist in the real material, which makes the defect structures much more complicated. Nevertheless, the predominant defect is the same for both configurations, namely the Barium Frenkel defect. However, the distribution of Mg changes the defect properties; the most significant change is in the oxygen interstitial position. The Mg distribution that retains the mirror symmetry in the barium-oxygen plane constrains the oxygen interstitial ion in the mirror plane to form a two-bridge configuration instead of a Reidinger defect, as in β-alumina. However, if the Mg distribution destroys the mirror symmetry, the oxygen will stay inside the spinel block in the half unit cell without Mg. It seems that the relative charge of Mg'_{Al} plays an important role in determining the positions of defects. Both the two-bridge and Reidinger defect structures are likely to co-exist.

Two sets of potential models have been tested. The results show a predicted difference in the predominant thermal defect, but the europium defects had the same properties. Two low-energy europium sites were found: divalent ions prefer to occupy the Beevers-Ross site in the mirror plane while trivalent europium ions prefer the Al(2) tetrahedral position in the spinel block. Although the calculated Eu^{3+}—O bond length is smaller than the expected value, the difference is small and the bond valence sum is in the reasonable range.

Defect complexes with two and three defects, at least one of which is Eu^{3+}, have been calculated and compared. The defect complexes did show smaller defect energies than the sum of individual defects, but the size of the decrease was not large enough to stabilize the Eu^{3+} ion in the mirror plane.

Although Eu^{3+} was predicted to prefer the Al site, this is a thermodynamic conclusion, and kinetic factors were not considered. For example, if Eu^{3+} was formed during use, by oxidation from Eu^{2+}, it would not be necessary for it to be at the Al(2) site. As the Eu^{2+} ion resides at the BR position in the conduction plane, Eu^{3+} could be formed at that position. Thermodynamics would then drive it to move to the Al(2) site. There is about 5 Å distance between the BR and Al(2) sites. Whether Eu^{3+} ions can migrate such a distance is a kinetic problem that will be investigated in a subsequent paper.

Acknowledgments

References

1. M. Bettman and L.L. Terner, *Inorg. Chem.*, **10**(7), 1442 (1971).

2. N. Iyi, Z. Inoue, and S. Kimura, *J. Solid State Chem.*, **61**(2), 236 (1986).

3. G.A. Rankin and H.E. Merwin, *J. Am. Chem. Soc.*, **38**(3), 568 (1916).

4. W.L. Bragg, C. Gottfried, and J. West, *Z. Kristallogr.*, **77**(2) 255 (1931).

5. C.A. Beevers and M.A.S. Ross, *Z. Kristallogr.*, **97**(1), 59 (1937).

6. B.G. Dick and A.W. Overhauser, *Phys. Rev.*, **112**(1), 90 (1958).

7. J.G. Park and A.N. Cormack, *Philos. Mag.*, **73**(1), 21 (1996).

8. J.G. Park and A.N. Cormack, *J. Solid State Chem.*, **121**(1), 278 (1996).

9. G.V. Lewis and C.R.A. Catlow, *J. Phys. C: Solid State Phys.*, **18**(6), 1149 (1985).

10. T.S. Bush, J.D. Gale, C.R.A. Catlow, and P.D. Battle, *J. Mater. Chem.*, **4**(6), 831 (1994).

11. C.R.A. Catlow, A.N. Cormack, and F. Theobald, *Acta Crystallogr., Sect. B: Struct. Sci.*, **B40**(3), 195 (1984).

12. A.N. Cormack, *Solid State Ionics*, **8**(1), 187 (1983).

13. N.F. Mott and M.J. Littleton, *Trans. Faraday Soc.*, **34**(1), (1938).

14. W.L. Roth, F. Reidinger, and S.L. Placa, in *Superionic Conductors*, edited by G.D. Mahan and W.L. Roth (Plenum, New York, 1976), p. 223.

15. K. Edstrom and J.O. Thomas, *Acta Crystallogr., Sect. B: Struct. Sci.*, **B47**(2), 210 (1991).

16. A.N. Cormack, in *Advances in Solid-State Chemistry*, edited by C.R.A. Catlow (Jai Press, Greenwich, Connecticut, 1993), p. 63.

17. I.D. Brown, in *Structure and Bonding in Crystals*, edited by M. O'Keeffe and A. Navrotsky (Academic Press, New York, 1981), p. 1.

18. N.E. Brese and M. O'Keeffe, *Acta Crystallogr., Sect. B: Struct. Sci.*, **B47**(1), 192 (1991).